Analytica Chimica Acta 1136 (2020) 1–8

Contents lists available at ScienceDirect

Analytica Chimica Acta

journal homepage: www.elsevier.com/locate/aca

Ultrasensitive electrochemical biosensor for detection of microRNA-155 as a breast cancer risk factor

Fatemeh Hakimian [a, b], Hedayatollah Ghourchian [a, *]

[a] Institute of Biochemistry and Biophysics, University of Tehran, Tehran, P.O. Box 13145-1384, Iran
[b] Medical Nanotechnology & Tissue Engineering Research Center, Yazd Reproductive Sciences Institute, Shahid Sadoughi University of Medical Sciences, Yazd, Iran

HIGHLIGHTS

- A simple, cost-effective and highly sensitive electrochemical biosensor for detection of miR-155 in serum is presented.
- This sensor achieves an ultralow detection limit (20 zmol) and a wide dynamic range.
- Normal and cancerous serums were diagnosed by the biosensor successfully.

GRAPHICAL ABSTRACT

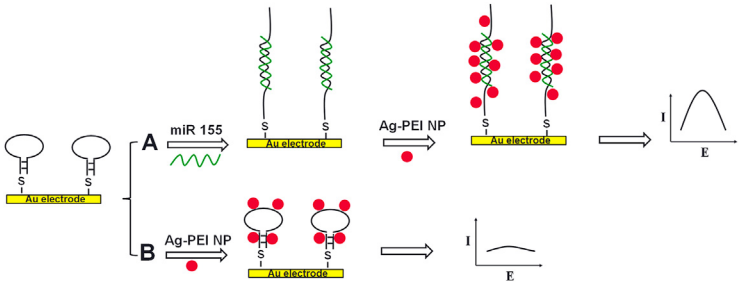

ARTICLE INFO

Article history:
Received 29 April 2020
Received in revised form
27 July 2020
Accepted 19 August 2020
Available online 28 August 2020

Keywords:
Polyethyleneimine
Silver nanoparticles
MicroRNA-155
Breast cancer
Biosensor

ABSTRACT

Due to the stability of microRNAs (miRNAs) in serum and other body fluids, they are known as promising cancer biomarkers. Recent studies have indicated higher expression of miRNA-155 (miR-155) in patients with breast cancer compared to healthy people. In the present report, a rapid and sensitive electrochemical biosensor has been developed for detection of miR-155 as a breast cancer risk factor. At first, a thiolated probe was immobilized on the gold electrode surface. Then, the target (miR-155) was exposed to the probe. In the next step, the positively charged polyethyleneimine-silver nanoparticles as electroactive labels were absorbed onto the negatively charged probe-target hybrid. In the third step, the anodic peak current which was produced due to the oxidation of silver nanoparticles was recorded as the electrochemical signal. The designed biosensor provided an ultrasensitive method for the detection of miR-155 with the detection limit of 20 zmol and a wide linear range from 2×10^{-20} to 2×10^{-12} mol. Moreover, the biosensor was able to detect miR-155 in real serum samples with satisfactory results.

1. Introduction

Breast cancer is the most common cancer among women, and the second rank in cancer incidence worldwide [1,2]. So, early detection of breast cancer by screening is a key solution to reduce mortality (qi Chen et al., 2000). Mammography is currently used as a noninvasive method for breast cancer screening. However, this method suffers from the disadvantages including usual false-negative results, high rate of false-positive data, incurred cost and required expertise [3]; qi Chen et al., 2000). Therefore, emerging

* Corresponding author.
E-mail address: ghourchian@ut.ac.ir (H. Ghourchian).

https://doi.org/10.1016/j.aca.2020.08.039
0003-2670/

novel biomarkers such as miRNAs in body fluids plays an important role in breast cancer screening [4,5].

MiRNAs are a class of small endogenous non-coding RNAs that have been implicated in a number of different diseases, including cancer [6–9]. An important aspect of using miRNAs as a biomarker for cancer detection is their presence in body fluids such as blood, plasma, and serum [10]. The other positive features of miRNAs as biomarker are their stability even at low or high pH, high temperature, long-time storage at room temperature, and multiple freeze-thaw cycles [11–13]. In 2014, Zeng and coworkers understood that overexpression of miR-155 in the serum of breast cancer patients is adequate to be used as a biomarker for breast cancer screening [14,15]. It was also reported that overexpression of miR-155 in breast cancer cells strengthens the cell proliferation and tumor formation through the repression of target genes such as Socs1 and RhoA [16–18]. In addition, it was shown that reducing miR-155 concentration after surgery or chemotherapy indicates that miR-155 can be utilized as an indicator to control the treatment response and trend in patients with breast cancer [16,18]. The current methods for detection of miRNA are mainly included: reverse transcription polymerase chain reaction (RT-PCR) [19], northern blotting [20], microarray technique [21], and in situ hybridization [22]; Tian et al., 2015). Although these methods have some advantages, they suffer from requiring expensive instruments and reagents or labored labeling process. So, developing a rapid, simple, label-free, and cost-effective method for direct measurement of miR-155 in serum can be a valuable method for breast cancer screening [23–26]. So far, several biosensors have been reported for the precise detection of miRNA. They mostly utilized metallic nanoparticles as a redox-active indicator [27]. Pyrrolidinyl peptide nucleic acid-silver nanofoam electrodeposited on a gold electrode [28] and the nanoparticles synthesized onto DNA templates [29,30] are the examples of redox indicator utilized for signal amplification in biosensors.

In the present report, a sensitive electrochemical biosensor is introduced by using polyethyleneimine-silver nanoparticles (PEI-Ag NPs) as a redox-active indicator. The biosensor comprises a capture hairpin probe immobilized on the gold electrode surface. In the presence of the target (miR-155), hairpin structure is opened and negatively charged probe-target duplex is formed. Then, by addition of the electroactive and positively charged PEI-Ag NPs, a sharp electric peak current is produced which indicates miR-155 level.

2. Experimental section

2.1. Apparatus

Electrochemical measurements were performed using a potentiostat/galvanostat (Model 263A, EG&G, USA) controlled by a PowerSuite software package. All electrochemical experiments were carried out at room temperature in a conventional three-electrode system including a modified gold as a working electrode, a platinum wire as a counter electrode, and an Ag/AgCl (3 M KCl solution) as a reference electrode (from Azar Electrode, Urmia, Iran). UV–Vis absorption spectra were recorded using a Varian Cary Bio 100 spectrophotometer. The particles were characterized by dynamic light scattering (DLS) instrument (90 Plus Pals, Brookhaven Instruments Corp., USA), and PALS zeta-particle sizing potential analyzer software. The morphology of PEI-Ag NPs was studied by field emission scanning electron microscopy (FESEM) using a Tescan Mira3 XMU (Czech Republic). Also, the synthesized PEI-Ag NPs were analyzed by scanning electron microscopy (SEM; FEI Quanta 200) and energy-dispersive X-ray (EDX) microanalysis spectroscopy.

2.2. Materials

The HPLC purified oligonucleotide sequences utilized in the present research are as follows: Thiolated capture probe (5′-AAAAAAAAACCCCTATCACGATTAGCATTAATTTTTTTTT–HS–3′) was purchased from AnaSpec, Inc. (Canada). Hsa-miR-155 (5′-UUAAUGCUAAUCGUGAUAGGGGU-3′) and three-base mismatched hsa-miR-155 (5′-UUAAUGCUUAUCGAGAUACGGGU-3′) were synthesized by Bioneer Corporation (Republic of South Korea). Polyethylenimine (50% solution, M_n ~ 1200, M_w ~ 1300), $AgNO_3$, Diethylpyrocarbonate (DEPC), NaH_2PO_4, Na_2HPO_4, NaCl, and H_2SO_4 were purchased from Merck (Germany).

2.3. Synthesis of PEI-Ag NPs

PEI-Ag NPs were prepared according to the procedure reported in the literature [31] with slight modification. Briefly, 25 mL of 9 mM $AgNO_3$ and 5 μL of PEI (50% solution) is brought to boiling temperature while stirring vigorously. Boiling is continued for 15 min until the solution color changes from colorless to green-gray. Then, the mixture was centrifuged and decanted. Then, the precipitate was washed with deionized water followed by sonication for 1 min.

2.4. Capture probe design

To enhance the sensor specificity, capture probe was designed to form a hairpin (stem-and-loop) structure [32]. The loop consists of a probe sequence that is complementary to the target (miR-155). The stem sequence is independent of the target sequence. The stem contains nine thymidine nucleotides at 3′ end, which provides optimal immobilization and hybridization efficiency [33,34]. For covalent attachment of the capture probes onto the electrode surface, each probe molecule has a thiol group at 3′ terminus.

2.5. Probe immobilization and miR-155 measurement

Before modification, the gold working electrodes were polished with 10 μm and 5 nm alumina slurry sequentially and then rinsed with water. Then, gold electrodes were electrochemically cleaned by cycling between −0.4 and 1.6 V vs. Ag/AgCl in 0.5 M sulfuric acid until the cyclic voltammograms (CVs) becomes stable (approximately 20 cycles) [35,36]. Finally, the cleaned gold electrodes were washed with deionized water several times to ensure the removal of undesirable chemical species.

To attach the thiolated capture probe on the electrode surface, 8 μL of probe (1 μM) and 8 μL of phosphate-buffered saline (PBS) were mixed and dropped on the gold electrode. After drying for 30 min under an infrared lamp, the electrode rinsed three times with deionized water. In the next step, the modified gold electrode immersed into a solution composed of PBS 0.1 M at 60 °C for 30 s. Thereafter immediately, 2 μL of the target was mixed with 2 μL of PBS and then the mixture was dropped on the electrode surface to hybridize with the probe. Then, the electrode was dried under the infrared lamp and washed with deionized water. In the final step, the positively charged PEI-Ag NPs (1.8 μg suspended in 6 μL deionized water) were cast on the Au electrode surface to absorb onto the negatively charged probe-target hybrid. After drying and washing, the CV of the modified electrode was recorded in 2 mL of PBS (0.1 M) at the potential range from 0.6 to −0.6 V while the scan rate was 150 mV s^{-1}.

3. Results and discussion

3.1. Characterization of PEI-Ag NPs

The UV–Vis spectrum of PEI-Ag NPs is illustrated in Fig. 1A. The single absorption peak at ~400 nm is the characteristic peak attributed to the surface plasmon resonance band of the Ag colloid. This result is well-matched with that reported previously for Ag colloid [37–40]. To investigate the morphology of nanoparticles, FESEM was used. As seen in Fig. 1B, nanoparticles are nearly spherical in shape. The mean diameter and zeta potential of PEI-Ag NPs were measured by DLS to be 32.2 ± 0.5 nm and 46.24 ± 2.33 mV, respectively. The positive zeta potential of PEI-Ag NPs originates from the amine groups of polyethylenimine.

The elemental analysis of PEI-Ag NPs composition is carried out by EDX spectroscopy (Fig. 2). EDX data confirmed the presence of silver, carbon and nitrogen in the nanoparticles. Carbon and nitrogen peaks originate from polyethylenimine which composed of amine groups and carbon aliphatic CH_2CH_2 spacers. Al peaks are attributed to the aluminum foil used as the holder. Elemental mapping by EDX (Fig. 2) clearly shows the uniform distribution of the elements.

3.2. Electrochemical responses

Fig. 3 shows the CVs obtained for various modification steps in 0.1 M PBS buffer solution (pH 7.4) at the scan rate of 150 mV s^{-1}. The bare Au (curve a), Au-probe (curve b) and Au-probe/target (curve c) modified electrodes do not show a remarkable peak. But, Au-probe + PEI-Ag NPs (curve d) and Au-probe/target + PEI-Ag NPs (curve e) modified electrodes show very sharp redox current versus Ag/AgCl reference electrode. These peaks attributed to the redox behaviors of PEI-Ag NPs. According to the redox reaction 1, at electrode surface, the absorbed Ag NPs on polyethylenimine branches are oxidized to AgCl. This electrochemical process might be the main reason for the sharp redox peak produced by the biosensor (Fig. 3).

$$Ag + Cl^- \rightleftarrows AgCl + e^- \quad (1a)$$

So, it seems that the large surface area of polyethylenimine branches plays an important role for electron transferring process during the redox reaction 1 [41–43]. This redox reaction causes the anodic and cathodic peak potentials at 0.17 and −0.05 V, respectively (see Fig. 3) [41–43].

3.3. Detection mechanism

After cleansing the gold electrode, the capture probes were covalently attached to the electrode surface. Next, the target (miR-155) was introduced on the electrode and subsequently, the PEI-Ag NPs were dropped on the modified electrode (Scheme 1, A). In the presence of miR-155, the probe is hybridized with miR-155 and consequently, the DNA/RNA duplex is formed. By formation of the duplex, the negative charge density due to the presence of phosphate groups in the duplex backbone is increased. PEI-Ag NPs due to the presence of nitrogen atoms on PEI branches are highly positive. On the other hand, probe/miR-155 duplex has a more negative charge than the probe itself. So, positively charged PEI-Ag NPs are able to bind the probe/miR-155 duplex electrostatically more than those to the probe (Scheme 1, path A). In the absence of the target, the electrostatic interaction between the negative phosphate groups on hairpin structure and positive amine groups on PEI-Ag NPs is limited (Scheme 1, path B). As a result, in the presence of miR-155, further electrostatic absorption of nanoparticles leads to a stronger electrochemical response (Scheme 1).

3.4. Analytical approach of miRNA biosensor

In view of the fact that even in the absence of the target, a limited electrostatic interaction occurs between the negative phosphate groups on the hairpin probe and positive amine groups on PEI-Ag NPs (Scheme 1, path B) a background current is observed in all electrochemical measurements. On the other hand, due to any changes in probe immobilization conditions, this background current maybe differs from one to other electrodes. Consequently, this alteration in responses reduces the reproducibility of biosensor measurement results. To get rid of this background current and in order to make the results more reproducible, a relative current response (δI) was defined according to Equation (1) [33,44–46] and used as the electric current response of the biosensor.

$$\delta I = \left| \frac{I_{miR} - I_o}{I_{miR}} \right| \quad (1b)$$

where, I_{miR} and I_o indicate the amount of produced current in the presence and absence of miR-155, respectively. It is worth noting that all electric current responses (I_{miR} and I_o) are measured in the presence of PEI-Ag NPs. In Equation (1), the higher δI value indicates the presence of more concentration of miR-155 in the sample and consequently, more accumulation of PEI-Ag NPs on the modified electrode. Indeed, the concentration of miR-155 in the sample determines the probability of hybridizations between probe and target and formation of duplexes. Therefore, the higher negative charge of the duplex structure due to the phosphate groups increases the probability of PEI-Ag NPs binding through electrostatic interactions.

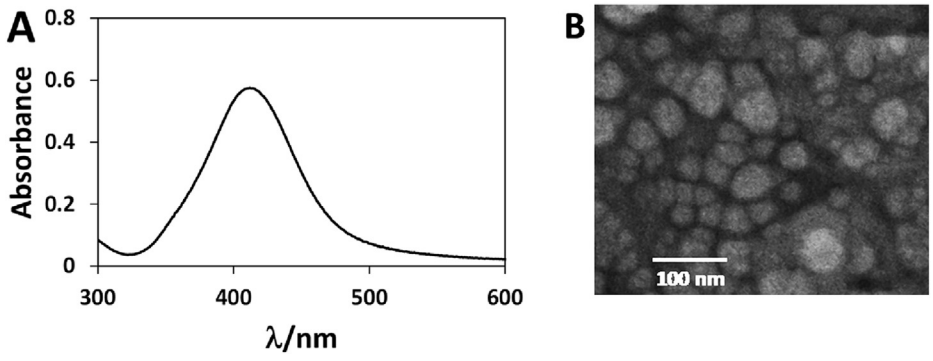

Fig. 1. UV–Vis absorption spectrum (A) and FESEM image (B) of the prepared PEI-Ag NPs.

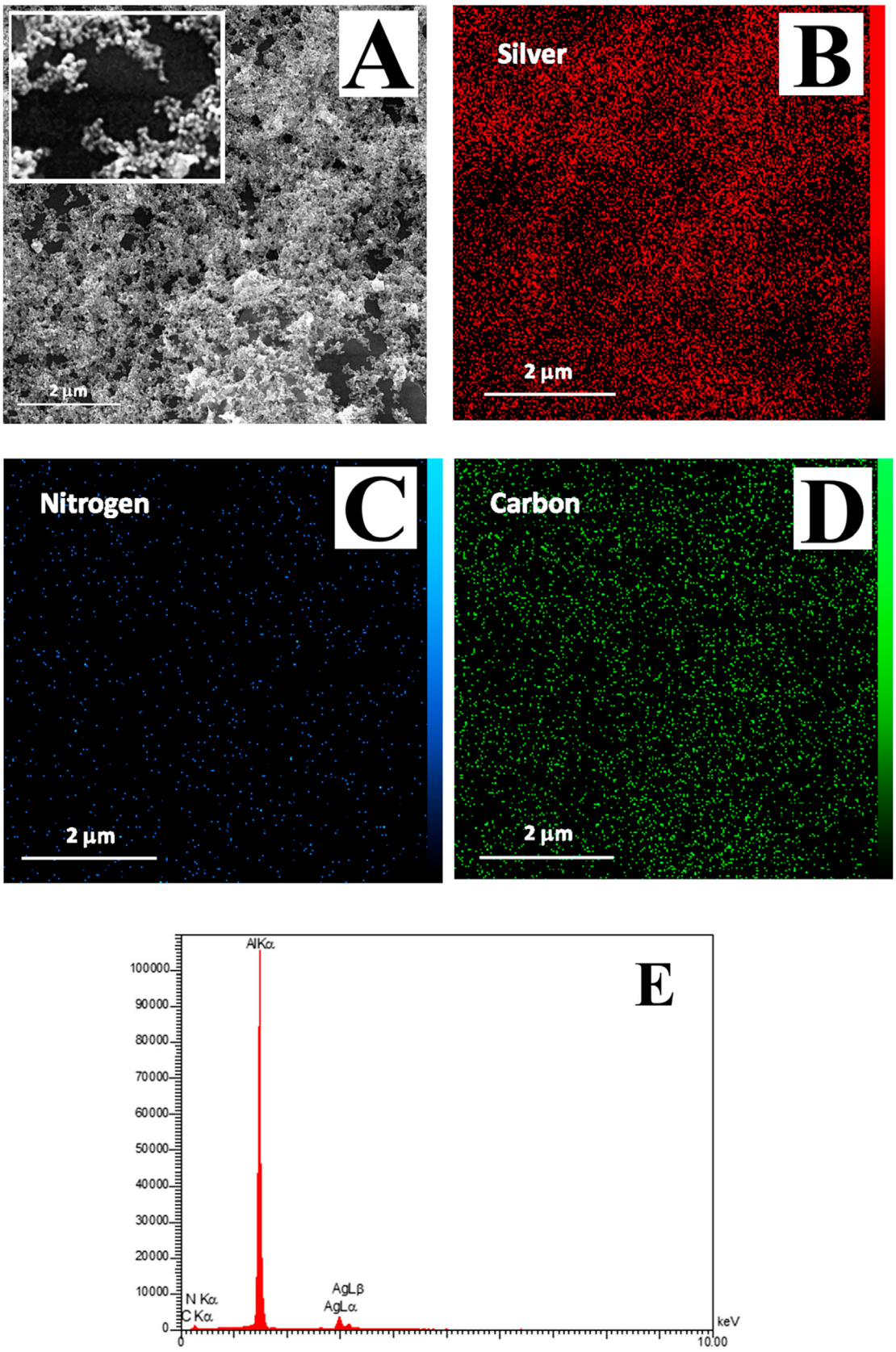

Fig. 2. SEM image; the inset shows the magnified image (A), corresponding EDX-based elemental mapping of silver (red) (B); nitrogen (blue) (C); carbon (green) (D), and EDX spectrum (E) of PEI-Ag NPs. (For interpretation of the references to color in this figure legend, the reader is referred to the Web version of this article.)

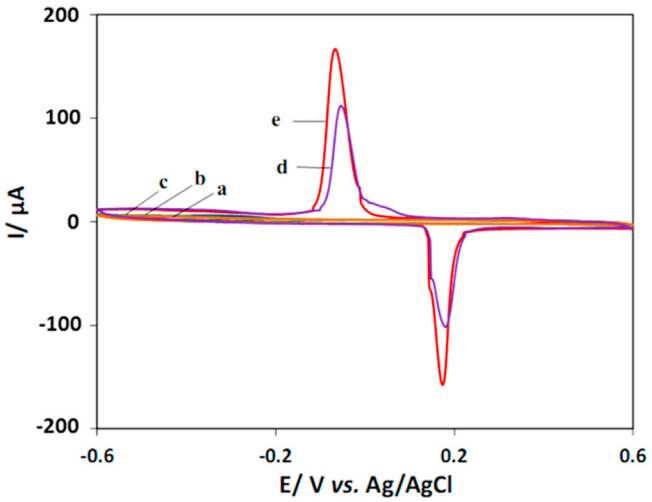

Fig. 3. CVs of different electrodes in 0.1 M PBS (pH 7.4) at the scan rate of 150 mV s^{-1}. a: Bare gold electrode. b: Thiolated capture probe immobilized on the gold electrode. c: The immobilized capture probe was hybridized with the complementary target (20 zmol). d: The immobilized capture probe electrostatically absorbed PEI-Ag NPs. e: The same as c, but after electrostatic interaction with PEI-Ag NPs. (For interpretation of the references to color in this figure legend, the reader is referred to the Web version of this article.)

Another factor that presumably contributes to the binding of nanoparticles to the duplex is more accessibility of phosphates negative groups on the duplex relative to those on single-stranded probe.

3.5. Optimization of biosensor performance

In order to optimize the probe concentration for the electrochemical biosensor, different concentrations of the probe (4, 8, 10, 20, and 40 pmol) were immobilized on the gold electrode surface. After addition of 20 pmol miR-155 on each concentration of the probe, in the presence of PEI-Ag NPs (1.8 μg), the CVs were recorded. As seen in Fig. 4A, the best δI was obtained for probe at a concentration of 8 pmol. At higher concentrations of 8 pmol, δI is decreasing. It seems that at high concentrations of probe, repulsive forces between negatively charged probe and miR-155 overcome the forces for probe-miR-155 hybridization.

For optimization of PEI-Ag NPs concentration, various amounts of PEI-Ag NPs (0.6, 1.2, 1.8, 3, and 3.6 μg) were dropped on the immobilized probe to form probe-target duplex. Then the CVs were recorded in phosphate-buffered saline (0.1 M, pH 7.4) at a scan rate of 150 mV/s. As seen in Fig. 4B, the best δI was obtained for PEI-Ag NPs at a concentration of 1.8 μg. It seems that at high concentrations of PEI-Ag NPs, the extra nanoparticles electrostatically absorbed on electrode surface and cause an extra current response relative to the signal produced by either probe alone, or probe-target hybrid. This is why the response (δI) obtained at PEI-Ag NPs concentration at above 1.8 μg is decreased gradually. It is necessary to mention that the next electrochemical measurements were carried out regarding the optimized concentrations of the probe and PEI-Ag NPs.

3.6. Calibration curve

To evaluate the analytical performance of the fabricated biosensor, a wide range of miR-155 concentrations from 2×10^{-11} to 2×10^{-22} mol were cast on the surface of modified electrode, and the resulting currents were measured at optimum condition. The obtained CVs are shown in Fig. 5A. It is worth noting that only anodic peak currents were utilized in this work due to their current reproducibility. The shift in anodic and cathodic peaks at higher miR-155 concentrations could be due to the PEI-Ag NPs accumulation on probe-target duplex and consequently the more availability of electroactive Ag NPs for redox reaction [47].

For the quantitative detection of miR-155, the linear range of the calibration curve (Fig. 5B) from 2×10^{-20} to 2×10^{-12} mol was used. Each point in the calibration curve is the mean value of three independent experiments. The interception of maximum and minimum slope at low concentrations of miR-155 limit was taken as limit of detection (LOD) [48–50]. By this method, 2×10^{-20} mol (20 zmol) were obtained as LOD. As compared in Table 1, this LOD is lower than those reported for other electrochemical biosensors. Such a low LOD may be due to the ability of the branched PEI to increase the surface area of interface (PEI branches/solution). This large interface perhaps facilitates the electronic communication between silver species (Ag ⇄ AgCl) and the electrode surface.

It is worth noting that in some cases a very slight splitting may occur on the peaks, similar to the anodic peaks in Figs. 3 and 5A. Moreover, in some extreme cases, the peak splitting improves so that the anodic peak may be divided into two peaks (data not shown). According to Ref. [56,57]; the existence of the heterogeneous electrode may cause such a splitting. Here, the distribution of PEI-Ag NPs on the modified electrode surface could be the reason for the heterogeneous electron transferring process. In addition, the formation of species such as silver hydroxide (AgOH) and silver oxide (Ag_2O) may also affect the peak splitting (Reactions 2 and 3)

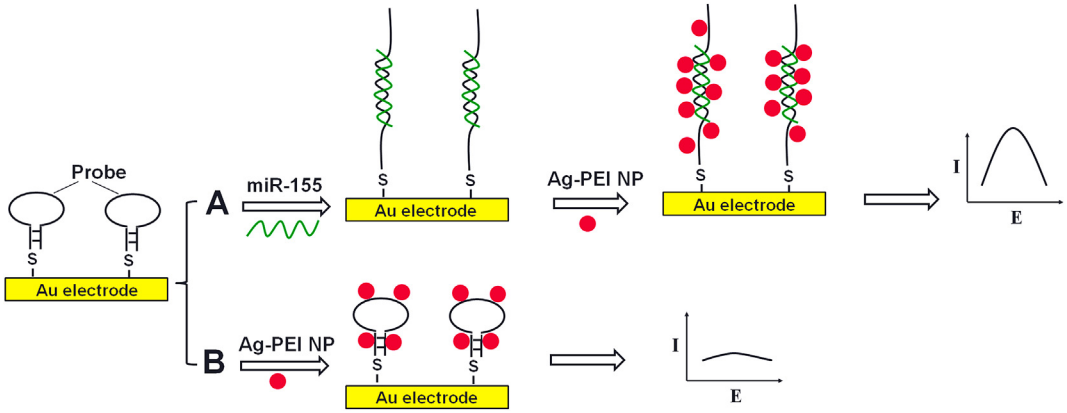

Scheme 1. Schematic illustration of fabrication the electrochemical biosensor.

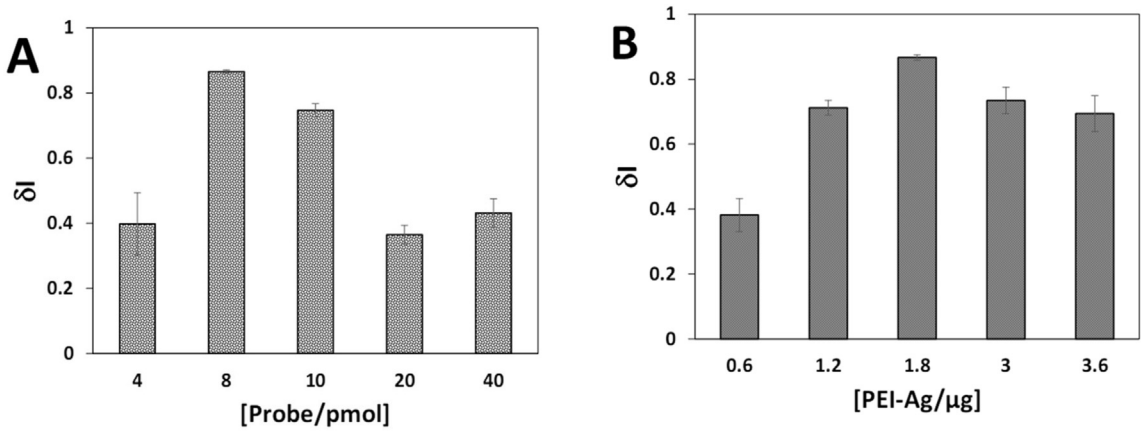

Fig. 4. Optimization of probe concentration (A) and the amount of PEI-Ag NPs (B) for electrochemical biosensor. Experiments were performed in 0.1 M phosphate-buffered saline (pH 7.4) and a scan rate of 150 mV/s. Each column indicates the mean value of three independent measurements.

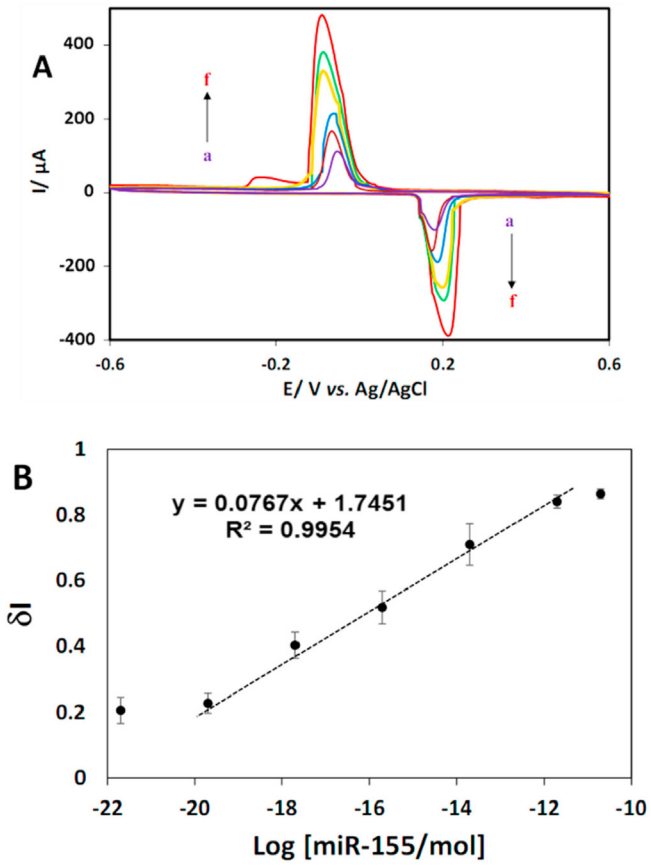

Fig. 5. A) The CVs obtained by the electrochemical biosensor at different concentrations of miR-155: a: 0, b: 2×10^{-22}, c: 2×10^{-20}, d: 2×10^{-18}, e: 10^{-16} and f: 10^{-14} mol. CVs were measured in 0.1 M PBS at a scan rate of 150 mV s^{-1}. B) Calibration curve for determination of miR-155. Each point indicates the mean value of three repetitive experiments.

[58,59].

$$Ag + OH^- \rightleftarrows AgOH + e^- \quad (2)$$

$$2Ag + 2OH^- \rightleftarrows Ag_2O + H_2O + 2e^- \quad (3)$$

It should be noted that as we examined, the PEI-Ag NPs as an electrochemical label is quite stable at 4 °C for at least 6 months. The thiolated capture probe immobilized on the gold electrode also is stable for about 1.5 months when stored at 4 °C (See Figs. 1S and 2S).

3.7. Specificity

The specificity of the biosensor was studied using two sequences including miR-155 (perfect complementary target) and three-base mismatched miR-155. A comparison of biosensor responses in the presence and absence (as control) of two sequences is shown in Fig. 6A. As seen, the biosensor response in the presence of miR-155 is almost two times that produced via three-base mismatch miR-155. This difference in the response indicates that duplex formation by probe/miR-155 (curve a) is more probable than that formed by probe/three-base mismatched miR-155 (curve b). Based on the CVs obtained for two samples, δI values was calculated to be 0.70 ± 0.01 and 0.56 ± 0.08 for miR-155 and three-base mismatched miR-155, respectively.

3.8. Real sample analysis

To demonstrate the capability of the biosensor for quantification of real samples, human clinical specimens (including cancerous and normal sera) were obtained from Shahid Sadoughi Hospital (Yazd, Iran) and analyzed. It should be noted that the ratio of serum and buffer is 1:1. This means that 50 μL of buffer was mixed with 50 μL of serum. Then, the serum samples must be heated for 15 min at 90–95 °C before usage to release miR-155 from the protective proteins. As seen in Fig. 6B, in the presence of cancerous serum a higher current is produced compared to that of normal serum. This indicates that in the case of the cancerous sample, more duplexes are formed, more PEI-Ag NPs bind to the modified electrode and higher current is produced. Based on the CVs obtained for 2 human clinical specimens, δI values was calculated to be 0.42 ± 0.08 and 0.71 ± 0.01 for normal and cancerous real specimens, respectively.

4. Conclusions

In the present work, a versatile, simple, cost-effective and highly sensitive electrochemical biosensor has been developed for the detection of miR-155 as a biomarker for breast cancer screening. Using this biosensor an ultralow detection limit and a wide dynamic range were achieved. Such characteristics may be attributed

Table 1
Comparison between different electrochemical sensors for RNA detection.

Strategy	Target	Linear range	LOD	Ref.
Based on PEI-Ag NPs	miR-155	20 zmol-2 pmol	20 zmol	This study
Based on a pyrrolidinyl peptide nucleic acid/polypyrrole/silver nanofoam	miR-21	0.20 fM-1.0 nM	0.20 fM	[28]
Based on copper nanoclusters	miR-21	0.1 fM-10 pM	10 aM	[29]
Based on silver nanoclusters	miR-199a	1.0 fM-0.1 nM	0.64 fM	[30]
Triple-stem DNA redox probe structure	miR-122	–	0.1 fM	[9]
Based on Atomic force microscopy	miR-155	1 fM-100 pM	5.7 aM	[16]
Guanine oxidation consequent to the hybrid formation	miR-122	–	0.1 pmol	[51]
Tetrahedron-based/HRP	miR-21	–	10 fM	[52]
MoS_2 nanosheet modified with thionine and gold nanoparticles	miR-21	1 pM-10 nM	0.26 pM	[53]
Ternary SAM assembly/HRP/TMB	16S rRNA	–	40 zmol	[54]
Based on naphthalene sulfonic acid	miR-21	10 fM-10 nM	20 fM	[55]
Based on a duplex-specific nuclease	let-7b	2 fM-2 pM	1 fM	(Ren et al., 2013)

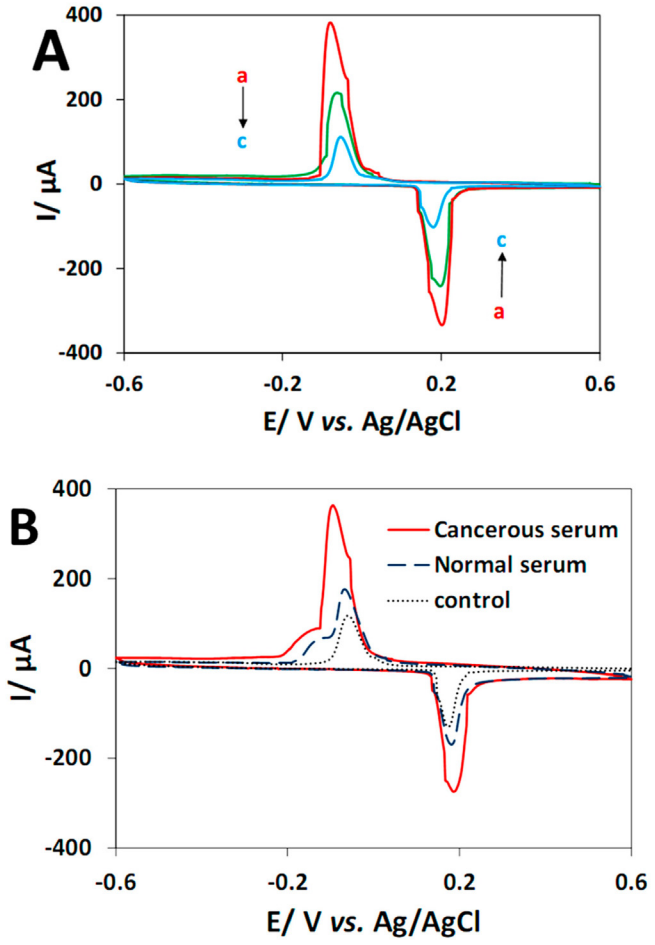

Fig. 6. A) The specificity of biosensor response toward miR-155. The CVs of c: Immobilized probe; b: Hybrids with the three-base mismatched target; a: Hybrids with fully complementary target. All of the CVs were recorded after PEI-Ag NPs addition in PBS buffer solution at a scan rate of 150 mV s^{-1}. B) Biosensor responses to cancerous and normal human serum samples. Control shows biosensor response toward immobilized probe after PEI-Ag NPs addition.

to the role of branched PEI in the enhancement of trapped Ag NPs which followed by AgCl formation on the PEI branches during CV scans. Moreover, successful diagnosing of the normal and cancerous specimens revealed that the biosensor has the potential to be used for screening breast cancer in biomedical research and clinical point of care applications.

CRediT authorship contribution statement

Fatemeh Hakimian: Doing experiments, Writing - original draft. **Hedayatollah Ghourchian:** Supervision, Writing - review & editing.

Declaration of competing interest

The authors declare that they have no known competing financial interests or personal relationships that could have appeared to influence the work reported in this paper.

Acknowledgement

Financial supports provided by the Research Council of the University of Tehran are gratefully appreciated. The authors also thank Dr. Hadi Zare-Zardini of Shahid Sadoughi Hospital for preparing the serum samples.

Appendix A. Supplementary data

Supplementary data to this article can be found online at https://doi.org/10.1016/j.aca.2020.08.039.

References

[1] J. Ferlay, I. Soerjomataram, R. Dikshit, S. Eser, C. Mathers, M. Rebelo, D.M. Parkin, D. Forman, F. Bray, Int. J. Canc. 136 (2015) E359–E386.
[2] M. Ghoncheh, Z. Pournamdar, H. Salehiniya, Asian Pac. J. Canc. Prev. 17 (2016) 43–46.
[3] E.K. Ng, R. Li, V.Y. Shin, H.C. Jin, C.P. Leung, E.S. Ma, R. Pang, D. Chua, K.M. Chu, W. Law, PloS One 8 (2013) 1–10.
[4] F. Biagioni, N. Bossel Ben-Moshe, G. Fontemaggi, Y. Yarden, E. Domany, G. Blandino, Cell Cycle 12 (2013) 2371–2375.
[5] V. De Guire, R. Robitaille, N. Tetreault, R. Guerin, C. Menard, N. Bambace, P. Sapieha, Clin. Biochem. 46 (2013) 846–860.
[6] H. Dong, J. Zhang, H. Ju, H. Lu, S. Wang, S. Jin, K. Hao, H. Du, X. Zhang, Anal. Chem. 84 (2012) 4587–4593.
[7] A. Grishok, A.E. Pasquinelli, D. Conte, N. Li, S. Parrish, I. Ha, D.L. Baillie, A. Fire, G. Ruvkun, C.C. Mello, Cell 106 (2001) 23–34.
[8] M. Lagos-Quintana, R. Rauhut, W. Lendeckel, T. Tuschl, Science 294 (2001) 853–858.
[9] T. Wang, E. Viennois, D. Merlin, G. Wang, Anal. Chem. 87 (2015) 8173–8180.
[10] R. Fiammengo, Biomarkers Med. 11 (2017) 69–86.
[11] E.E. Creemers, A.J. Tijsen, Y.M. Pinto, Circ. Res. 110 (2012) 483–495.
[12] C.H. Lawrie, S. Gal, H.M. Dunlop, B. Pushkaran, A.P. Liggins, K. Pulford, A.H. Banham, F. Pezzella, J. Boultwood, J.S. Wainscoat, Br. J. Haematol. 141 (2008) 672–675.
[13] P.S. Mitchell, R.K. Parkin, E.M. Kroh, B.R. Fritz, S.K. Wyman, E.L. Pogosova-Agadjanyan, A. Peterson, J. Noteboom, K.C. O'Briant, A. Allen, Proc. Natl. Acad. Sci. Unit. States Am. 105 (2008) 10513–10518.
[14] S.L. Anwar, D.S. Tanjung, M.S. Fitria, A.I. Kartika, D.N.I. Sari, D. Rakhmina, T. Wardana, I. Astuti, S.M. Haryana, T. Aryandono, Asian Pac. J. Canc. Prev. APJCP 21 (2020) 491–497.
[15] H. Zeng, C. Fang, S. Nam, Q. Cai, X. Long, BioMed Res. Int. (2014) 1–7, 2014.
[16] A.R. Cardoso, F.T. Moreira, R. Fernandes, M.G.F. Sales, Biosens. Bioelectron. 80

(2016) 621–630.
[17] S. Jiang, H.W. Zhang, M.H. Lu, X.H. He, Y. Li, H. Gu, M.F. Liu, E.D. Wang, Canc. Res. 70 (2010) 3119–3127.
[18] Y. Sun, M. Wang, G. Lin, S. Sun, X. Li, J. Qi, J. Li, PloS One 7 (2012) 1–8.
[19] E. Varkonyi-Gasic, R. Wu, M. Wood, E.F. Walton, R.P. Hellens, Plant Methods 3 (2007) 1–12.
[20] E. Várallyay, J. Burgyán, Z. Havelda, Nat. Protoc. 3 (2008) 190–196.
[21] W. Li, K. Ruan, Anal. Bioanal. Chem. 394 (2009) 1117–1124.
[22] M. Deo, J.Y. Yu, K.H. Chung, M. Tippens, D.L. Turner, Dev. Dynam. 235 (2006) 2538–2548.
[23] C. Fan, K.W. Plaxco, A.J. Heeger, Proc. Natl. Acad. Sci. Unit. States Am. 100 (2003) 9134–9137.
[24] Y. Mao, C. Luo, Q. Ouyang, Nucleic Acids Res. 31 (2003) 1–6.
[25] Y. Zhou, M. Wang, X. Meng, H. Yin, S. Ai, RSC Adv. 2 (2012) 7140–7145.
[26] X. Wu, Y. Chai, P. Zhang, R. Yuan, ACS Appl. Mater. Interfaces 7 (2014) 713–720.
[27] P. Gillespie, S. Ladame, D. O'Hare, Analyst 144 (2019) 114–129.
[28] T. Kangkamano, A. Numnuam, W. Limbut, P. Kanatharana, T. Vilaivan, P. Thavarungkul, Biosens. Bioelectron. 102 (2018) 217–225.
[29] Y. Wang, X. Zhang, L. Zhao, T. Bao, W. Wen, X. Zhang, S. Wang, Biosens. Bioelectron. 98 (2017) 386–391.
[30] C. Yang, K. Shi, B. Dou, Y. Xiang, Y. Chai, R. Yuan, ACS Appl. Mater. Interfaces 7 (2015) 1188–1193.
[31] K. Kim, J.W. Lee, K.S. Shin, ACS Appl. Mater. Interfaces 4 (2012) 5498–5504.
[32] Y.E. Khudyakov, H.A. Fields, Artificial DNA: Methods and Applications, CRC Press, 2002.
[33] F. Hakimian, H. Ghourchian, A.S. Hashemi, M.R. Arastoo, M.B. Rad, Sci. Rep. 8 (2018) 2943.
[34] C. Pöhlmann, M. Sprinzl, Anal. Chem. 82 (2010) 4434–4440.
[35] L.M. Fischer, M. Tenje, A.R. Heiskanen, N. Masuda, J. Castillo, A. Bentien, J. Émneus, M.H. Jakobsen, A. Boisen, Microelectron. Eng. 86 (2009) 1282–1285.
[36] J.Y. Gerasimov, R.Y. Lai, Chem. Commun. 47 (2011) 8688–8690.
[37] C. Aymonier, U. Schlotterbeck, L. Antonietti, P. Zacharias, R. Thomann, J.C. Tiller, S. Mecking, Chem. Commun. (2002) 3018–3019.
[38] Z. Liu, Y. Wang, Y. Zu, Y. Fu, N. Li, N. Guo, R. Liu, Y. Zhang, Mater. Sci. Eng. C 42 (2014) 31–37.
[39] Z. Liu, Z. Xing, Y. Zu, S. Tan, L. Zhao, Z. Zhou, T. Sun, Mater. Sci. Eng. C 32 (2012) 811–816.
[40] Y. Zhang, H. Peng, W. Huang, Y. Zhou, X. Zhang, D. Yan, J. Phys. Chem. C 112 (2008) 2330–2336.
[41] Y.J. Choi, T.J.M. Luo, Int. J. Electrochem. (2011) 1–6, 2011.
[42] Z.J. Jiang, C.Y. Liu, Y.J. Li, Chem. Lett. 33 (2004) 498–499.
[43] X. Pei, Z. Xu, J. Zhang, Z. Liu, J. Tian, Anal. Methods 5 (2013) 3235–3241.
[44] D. Gentili, P. D'Angelo, F. Militano, R. Mazzei, T. Poerio, M. Brucale, G. Tarabella, S. Bonetti, S.L. Marasso, M. Cocuzza, J. Mater. Chem. B 6 (2018) 5400–5406.
[45] B. Piro, S. Reisberg, G. Anquetin, H.-T. Duc, M.-C. Pham, Biosensors 3 (2013) 58–76.
[46] F. Zhao, X. Li, W. Xu, W. Zhang, X. Ying, Anal. Lett. 47 (2014) 1712–1725.
[47] A.J. Bard, L.R. Faulkner, J. Leddy, C.G. Zoski, Electrochemical Methods: Fundamentals and Applications, wiley, New York, 1980.
[48] R.P. Buck, E. Lindner, Pure Appl. Chem. 66 (1994) 2527–2536.
[49] S. Dawan, R. Wannapob, P. Kanatharana, W. Limbut, A. Numnuam, S. Samanman, P. Thavarungkul, Electrochim. Acta 111 (2013) 374–383.
[50] F.S. Mohammed, S.R. Cole, C.L. Kitchens, ACS Sustain. Chem. Eng. 1 (2013) 826–832.
[51] E. Lusi, M. Passamano, P. Guarascio, A. Scarpa, L. Schiavo, Anal. Chem. 81 (2009) 2819–2822.
[52] Y. Wen, H. Pei, Y. Shen, J. Xi, M. Lin, N. Lu, X. Shen, J. Li, C. Fan, Sci. Rep. 2 (2012) 1–6.
[53] D. Zhu, W. Liu, D. Zhao, Q. Hao, J. Li, J. Huang, J. Shi, J. Chao, S. Su, L. Wang, ACS Appl. Mater. Interfaces 9 (2017) 35597–35603.
[54] J. Wu, S. Campuzano, C. Halford, D.A. Haake, J. Wang, Anal. Chem. 82 (2010) 8830–8837.
[55] D.A. Smith, L.J. Newbury, G. Drago, T. Bowen, J.E. Redman, Sensor. Actuator. B Chem. 253 (2017) 335–341.
[56] K.R. Ward, N.S. Lawrence, R.S. Hartshorne, R.G. Compton, J. Phys. Chem. C 115 (2011) 11204–11215.
[57] K.R. Ward, N.S. Lawrence, R.S. Hartshorne, R.G. Compton, Phys. Chem. Chem. Phys. 14 (2012) 7264–7275.
[58] A. Habekost, World J. Chem. Educ. 4 (2016) 4–12.
[59] A. Safavi, M. Tohidi, Anal. Methods 4 (2012) 2233–2241.